CORE
Metadata, citation and similar papers at core.ac.uk
Provided by NASA Technical Reports Server

NASA Technical Memorandum 100616

A FINITE-ELEMENT ALTERNATING METHOD FOR TWO-DIMENSIONAL MODE-I CRACK CONFIGURATIONS

(NASA-TM-100616) A FINITE-ELEMENT ALTERNATING METHOD FOR TWO-DIMENSIONAL MODE-1 CRACK CONFIGURATIONS (NASA) 48 p CSCL 20K
N88-23276
Unclas
G3/39 0145734

I. S. Raju and W. B. Fichter

May 1988

National Aeronautics and Space Administration

Langley Research Center
Hampton, Virginia 23665

A FINITE-ELEMENT ALTERNATING METHOD FOR TWO-DIMENSIONAL MODE-I CRACK CONFIGURATIONS

I. S. Raju
Analytical Services and Materials, Inc.,
Hampton, Va.

and

W. B. Fichter
NASA Langley Research Center
Hampton, Va.

SUMMARY

A finite-element alternating method is presented for two-dimensional mode-I crack problems. An analytical solution for an arbitrary polynomial normal pressure distribution applied to the crack faces is obtained and used as the basic solution in the method. The method is applied to several crack problems to study its efficiency and the results are compared to accurate stress-intensity factor solutions in the literature. The method gave reasonably accurate stress-intensity factors and crack opening displacements with minimal computing effort. Because the method must model only the uncracked body, finite-element models with many degrees of freedom are not warranted and therefore, the method has been implemented on personal computers.

INTRODUCTION

Damage tolerant design concepts for aerospace structural components

are widely used to avoid catastrophic failures during service. Stress-intensity factors are important parameters in these designs, because they are necessary to predict fatigue crack growth rates and fracture strengths.

In two-dimensional analyses, several methods are available to calculate the stress-intensity factors of cracked components. Several stress-intensity factor compendia [1-4] are also available. However, there are always situations where the stress-intensity factor for a particular crack configuration and loading is not readily available and some approximations and estimates need to be made. Therefore, the search for algorithms, new methods and computer programs that are fast, accurate and efficient continues.

Recent literature shows that the finite-element alternating method (FEAM) is a powerful, accurate and computationally efficient [5-8] method for three-dimensional (3-D) analysis. This method was successfully applied to embedded-, surface-, and corner-cracked solids with elliptic or part-elliptic cracks. The method is based on the Schwartz-Neumann alternating method [9,10], a numerical method that alternates between two solutions to satisfy the required boundary conditions. Solution 1 is usually a continuum solution for a cracked infinite plate or solid. Solution 2 uses a numerical method such as the finite element method to model and analyze the uncracked plate or solid with the same configuration. The method alternates between these solutions to satisfy the required boundary conditions of the original problem. The 3-D FEAM was shown to be very efficient from the modeling point of view and also gives accurate stress-intensity factors [4-8]. The method is also more economical than the conventional finite-element method. Judging from the performance of the 3-D FEAM, a two-dimensional (2-

D) version of the method appears to be desirable. The purpose of the paper is to develop a 2-D version of FEAM, test the feasibility of using the method on personal computers, and study its efficiency by applying it to various crack configurations under mode-I loading.

First, the analytical solution for a crack in an infinite plate subjected to arbitrary crack face pressures is obtained. Next, the details of the FEAM are presented. Third, FEAM is applied to two-dimensional crack configurations for which exact or accurate solutions are available, to study the accuracy of the stress-intensity factors produced by the method. Several computational aspects of the method are also discussed.

LIST OF SYMBOLS

a	half-length or length of crack
F_I	normalized stress-intensity factor
H	half-height of plate
I_R	integral of residual norm defined in Equation (25)
K	mode-I stress-intensity factor
ℓ_j	length of j^{th} element along region of crack or external boundary
p_y	pressure distribution applied to crack faces
P	two symmetric concentrated loads on crack faces at a distance s from center of crack
N_c	number of elements along crack boundary
n_x, n_y	direction cosines of normal to boundaries along x- and y- directions, respectively
S	remote uniform applied stress

u,v	displacements in x- and y- directions, respectively
W	half-width or width of plate
x,y	Cartesian coordinates
z	complex variable, $z = x + iy$, $i = (-1)^{1/2}$

Matrices

$\{A\}$	coefficients of polynomial residual pressure distributions
$[K]$	assembled stiffness matrix of finite-element model
$\{Q^j\}$	assembled load vector for j^{th} iteration
$\{u^j\}$	finite-element displacement vector for j^{th} iteration

Greek Letters

δ	crack opening displacement at center of crack, (z=0).
Δ_I	maximum normalized crack opening displacement, $\Delta_I = E\delta/[4(1-\nu^2)Sa]$
$\{\sigma\}$	Cartesian stresses $\{ \sigma_x \quad \sigma_y \quad \sigma_{xy} \}^T$
ψ	Westergaard stress function, $\tilde{\psi} = \int \psi \, dz$, $\psi' = \frac{d\psi}{dz}$
μ	shear modulus
ν	Poisson's ratio

Superscripts

T	denotes transpose of a matrix
j	j^{th} iteration

ANALYTICAL SOLUTION

Consider an infinite plate with a crack of length 2a as shown in Figure 1. Use of the alternating method requires the solution for stresses and displacements everywhere in the plate due to an arbitrary polynomial

pressure distribution, p_y, applied to the crack faces. The applied polynomial pressure distribution is assumed to be of the form

$$p_y = \sum_{n=0}^{N} A_n (x/a)^n \tag{1}$$

To obtain the stresses and displacements everywhere in the infinite plate due to this arbitrary pressure distribution, the analytical solution for a typical term, $(x/a)^n$, must be obtained. To do this, consider the solution for a pair of normal forces P acting on the crack faces at a distance s from the center of the crack as shown in Figure 2. The Westergaard stress function, ψ_P, is [1]

$$\psi_P = \frac{P}{\pi (z-s)} \frac{(a^2-s^2)^{1/2}}{(z^2-a^2)^{1/2}} \tag{2}$$

where $z = x + iy$.

Using ψ_P as a Green's function, the stress function ψ for an arbitrary pressure distribution of Equation (1) is given by

$$\psi = \frac{1}{\pi a^n (z^2-a^2)^{1/2}} \int_{-a}^{a} (s^n (a^2 - s^2)^{1/2})/(z-s)\, ds \tag{3}$$

The singular integral in Equation (3) is of the form

$$I_n(z) = \int_{-a}^{a} (s^n (a^2 - s^2)^{1/2})/(s-z)\, ds \tag{4}$$

Integration over a contour enclosing the crack gives

$$I_n(z) = \pi [z^n (z^2-a^2)^{1/2} - G_\infty(z)] \tag{5}$$

where $G_\infty(z)$ is the principal part of $(z^{n+1} (1 - a^2/z^2)^{1/2})$ at $z = \infty$ [11].

The $G_\infty(z)$ in Equation (5) can be conveniently expressed for odd and even values of n as

$$G_\infty^{o}(z) = z^{2m+2} \sum_{k=0}^{m+1} C_k \left(-a^2/z^2 \right)^k / k! \qquad (6)$$

when $n = 2m+1$,

$$G_\infty^{e}(z) = z^{2m+1} \sum_{k=0}^{m} C_k \left(-a^2/z^2 \right)^k / k! \qquad (7)$$

when $n = 2m$, and

$$C_k = \begin{cases} 1 & \text{for } k = 0, \\ (1/2)\ (1/2-1)\ (1/2-2)\ \ldots\ (1/2-k+1) & \text{for } k=1,2,3\ldots \end{cases} \qquad (8)$$

The stress function in Equation (3) for any integer power n can then be written as

$$\psi(z) = \begin{cases} -\ (z/a)^n + G_\infty^{o}(z)/[\ a^n\ (z^2 - a^2)^{1/2}\ ], & \text{for odd } n \\ -\ (z/a)^n + G_\infty^{e}(z)/[\ a^n\ (z^2 - a^2)^{1/2}\ ], & \text{for even } n. \end{cases} \qquad (9)$$

The stresses at any location z in the plate are given by

$$\begin{aligned} \sigma_x &= \mathrm{Re}\ (\psi) - y\ \mathrm{Im}(\psi') \\ \sigma_y &= \mathrm{Re}\ (\psi) + y\ \mathrm{Im}(\psi') \\ \sigma_{xy} &= -\ y\ \mathrm{Re}(\psi') \end{aligned} \qquad (10)$$

where Re( ) and Im( ) denote the real and imaginary parts, respectively, of the function in the parentheses, and

$$\psi' = \frac{d\psi}{dz} \qquad (11)$$

The stress-intensity factors are given by

$$K = (2\pi)^{1/2} \lim_{z \to a} (z-a)^{1/2}\ \psi(z) \qquad (12a)$$

for the crack tip at $x = a$, and

$$K = (2\pi)^{1/2} \lim_{z \to -a} (-i)(z+a)^{1/2} \psi(z) \qquad (12b)$$

for the crack tip at x = -a.

The stress-intensity factors for each of the distributions $(x/a)^n$ have been computed for n=1 to 8, and are presented in Table 1. These results agree identically with those obtained by Isida [11] and given in reference 4 (page 189) for n= 0 to 3.

The displacements at any point z can also be obtained from the Westergaard stress function as

$$2\mu u = (1-2\nu)\ \mathrm{Re}\ (\tilde{\psi}) - y\ \mathrm{Im}\ (\psi)$$

$$2\mu v = 2(1-\nu)\ \mathrm{Im}\ (\tilde{\psi}) - y\ \mathrm{Re}\ (\psi) \qquad (13)$$

for plane strain. In Equation (13) μ is the shear modulus, ν is the Poisson's ratio and

$$\tilde{\psi} = \int \psi\, dz$$

For plane stress conditions, ν is replaced by $\nu/(1+\nu)$ in Equation (13).

The integrations involved in Equation (13) are straightforward and explicit expressions are not presented here. The maximum crack opening displacements, δ, at z=0 were obtained for each of the terms $(x/a)^n$ and are presented in Table 1.

FINITE-ELEMENT ALTERNATING METHOD

As previously mentioned, this method alternates between two solutions to satisfy the boundary conditions of the problem. Solution 1 is for an infinite plate with a crack subjected to arbitrary pressure distribution (Equations 9 and 10). Here for solution 2 the finite-element method is used. The procedure that is followed by the FEAM is given in reference 5 and is summarized here and in Figure 2 for completeness.

Step 1. Analyze the same configuration and loading as in the given problem, but without the crack, using the finite-element method.

Step 2. The finite-element method gives the stresses everywhere in the plate including the line segment coincident with the crack in the original problem. Because only mode-I configurations are considered here, no shear stresses σ_{xy} are present on the crack line.

Step 3. If the tractions on the crack faces are negligibly small (i.e. smaller than a prescribed tolerance level), stop and calculate the sum of the stress-intensity factors computed so far. If the tractions are not negligible go to step 4.

Step 4. To free the tractions on the crack faces, the crack face normal tractions, p_y, computed in step 3, must be erased. To do this, the negative of crack-face normal tractions (that is, $p_y^R = -p_y$) are applied in the analytical solution. The tractions p_y^R are expressed in polynomial form as

$$p_y^R(x) = \sum_{n=0}^{N} A_n (x/a)^n = \{P\}^T\{A\}$$

$$\text{where } \{P\}^T = \{1 \quad (x/a) \quad (x/a)^2 \quad . \quad . \quad . \quad (x/a)^N \}^T \tag{14}$$

The coefficients $\{A\}$ in Equation (14) are then calculated using a least squares procedure by

$$\{A\} = [H]^{-1} \{D\} \tag{15}$$

where

$$[H] = \sum_{j=1}^{N_c} \int_{\ell_j} \{P\}^T\{P\} \, dx \tag{16}$$

$$\{D\} = \sum_{j=1}^{N_c} \int_{\ell_j} \{P\}^T \, p_y^R(x) \, dx \tag{17}$$

where N_c = number of elements and ℓ_j is the length of the j^{th} element along the region of the crack. The integrals involved in Equations 16 and 17 are evaluated by Gaussian quadrature because discrete values of $p_y^R(x)$ are available in each of the N_c elements.

Step 5. The coefficients (A) determined in Equation (15) are then used to calculate the stress-intensity factors for the current (i^{th}) iteration, K^i, from

$$K^i = \sum_{n=1}^{N} (k_w)_n \, A_n^i \tag{18}$$

where $(k_w)_n$ are the stress-intensity factor weights given in Table 1 for each of the polynomial functions $(x/a)^n$.

Step 6. The crack face normal tractions p_y^R in step 4 create tractions on all the boundaries of the region of interest. These tractions are calculated for each of the polynomial functions by using Equations 9 and 10, at any point z on the boundary as

$$\underset{(3,1)}{\{\sigma\}} = \underset{(3,N)}{[M]} \; \underset{(N,1)}{\{A\}} \tag{19}$$

where

$$\{\sigma\}^T = \{\sigma_x \quad \sigma_y \quad \sigma_{xy}\}^T \tag{20}$$

and [M] are the tractions at any point z on the boundary due to unit values of each of the polynomial pressures. The normal (σ_n) and tangential (σ_t) tractions at any point on the boundaries of the region of interest are calculated by using

$$\{\sigma_n \quad \sigma_t\}^T = [q] \, \{\sigma\} \tag{21}$$

where

$$[q] = \begin{bmatrix} n_x & 0 & n_y \\ 0 & n_y & n_x \end{bmatrix} \tag{22}$$

where n_x, n_y are the direction cosines of the normal to the boundary with respect to the x and y axes, respectively.

Step 7. To satisfy the traction free boundary conditions the tractions created from step 6 by the residual pressures p_y^R on the crack face need to be erased. Therefore, the negative of these tractions are considered as the prescribed tractions for the finite-element model of the uncracked plate. They are conveniently expressed in terms of the nodal forces on each of the elements on the boundaries of the finite-element model by

$$\{Q\}_j = -[G]_j \{A\} \tag{23}$$

where

$$[G]_j = \int_{\ell_j} [N]^T [q] [M] \, ds \tag{24}$$

where the subscript j refers to the j^{th} element, [N] are the element shape functions, [q] is the direction cosine matrix in Equation (22), [M] is defined in Equation (19), and ℓ_j is the length of the side of element j on the boundary.

The nodal forces $\{Q\}_j$ on the j^{th} element on the external boundaries are treated as applied forces and are assembled to form a new load vector for the finite-element model of the uncracked body. Using this load vector, the uncracked body is analyzed once again (step 1). This is the start of the next iteration. The iterative process is continued until the crack face tractions in step 3 are negligibly small. In the converged solution, the stress-intensity factors are simply the sum of the stress-intensity factors for all iterations.

The criteria for convergence of the FEAM were formulated in terms of

the total magnitude of the crack face pressures and the incremental contributions to the stress-intensity factors. Define the integral of the residual normal tractions p_y^R in the region of the crack ℓ_c by

$$I_R^i = \int_{\ell_c} [\ p_y^R\ ]^i \, dx \qquad (25)$$

for the i^{th} iteration. If the integral I_R^{i+1} is greater than I_R^i and I_R^{i-1} the algorithm is terminated because of nonconvergence. The algorithm is continued as long as

$$I_R^{i+1} < I_R^i > I_R^{i-1} \text{ or,}$$

$$I_R^{i+1} < I_R^i < I_R^{i-1}$$

and is terminated when (I_R/I_R^1) is less than a predetermined tolerance.

Because the stress-intensity factors are sought by this method, the ratio of the absolute value of the stress-intensity factor increment from the current iteration i, to the sum of the stress-intensity factors computed so far can be used in a criterion for convergence as

$$r = K^i \Big/ \sum_{j=1}^{i-1} K^j < 0.01, \text{ for example.} \qquad (26)$$

Numerical experimentation showed that (I_R/I_R^1) is a better criterion than Equation (26) for monitoring the convergence and terminating the algorithm. This is because a choice of r=0.01 does not mean that the final stress-intensity factors are within one percent of the "true" stress-intensity factors. Therefore, the ratio (I_R/I_R^1) is used and when the ratio $(I_R/I_R^1) \leq 0.01$, the algorithm is terminated. The dependence of the final stress-intensity factors on the value of the ratio (I_R/I_R^1) used to terminate the algorithm is briefly examined later in the paper.

Obviously the stress-intensity factor solutions obtained by the

FEAM depends on the finite element mesh refinement for the uncracked plate. To ensure that the FEAM converges to the correct solution, at least two finite element models, coarse and fine, of the uncracked plate are desirable. This aspect also is examined in a later section of the paper.

Computational Aspects of the FEAM

In the finite element part of the method, the 8-noded isoparametric parabolic elements were used to model the uncracked body. Some computational aspects that make the method efficient are briefly discussed.

Decomposition of the Global Stiffness Matrix.- In the FEAM the uncracked body is analyzed by the finite-element method several times (the number of iterations required for convergence of stress-intensity factors) with a different load vector each time. Therefore, the finite-element stiffness equations can be written as

$$[K]\ \{u^0, u^1, u^2, \ldots\} = \{Q^0, Q^1, Q^2, \ldots\} \qquad (27)$$

where [K] is the assembled stiffness matrix, and $\{u^i\}$ is the displacement vector corresponding to the load vector $\{Q^i\}$ for the i^{th} iteration. Equation (27) can be very efficiently solved by finding the Cholesky factors of the stiffness matrix [K] soon after the stiffness matrix is assembled. This decomposition needs to be performed only once. Thereafter, the displacements $\{u^i\}$ for the load vector $\{Q^i\}$ can be obtained by back substitutions. The displacements $\{u^i\}$ can be obtained very inexpensively because the back substitutions consume far less CPU Time than the decomposition [4-8].

Boundary Tractions.- In step 7 of the method the nodal forces on each element on the boundaries are obtained. This computation can be

efficiently performed by calculating the [G] matrices in Equation (24) for all elements on the boundaries before the start of the first iteration. In each iteration only one matrix multiplication in Equation (23) is required for each element on the boundaries.

Stress Smoothing.- In step 2 of the method the distribution of p_y along the crack line is calculated from the finite-element solution. The nodal stresses computed in a finite-element solution can be inaccurate. Therefore, the stresses are computed at the 2x2 Gaussian points in an element and are extrapolated to the element nodes. (See references 12 and 13 for details on stress smoothing.)

Fictitious Pressures.- In the case of edge cracks, only one crack tip exists. The analytical solution used in the FEAM is based on an interior crack in an infinite plate. Therefore, to use the method for edge cracks, the crack face pressures were fitted onto the fictitious part of the crack which lies outside the analysis region. A simple linear extrapolation with p_y^R values at $x = 0$ and $x = a$ was used to obtain the values for $-a \leq x \leq 0$, as shown in Figure 3(a). This method is preferred over the extrapolation from a least-squares fit because extrapolation outside the analysis region is known to be inaccurate [5].

This concept of the fit in the region $-a \leq x \leq 0$ was also used from the view of computational convenience for crack configurations that are symmetric about the $y = 0$ line. For these configurations, only the even powers of n in the polynomial fit of Equation (14) for p_y^R need to be retained. However, it is convenient from a programming standpoint to retain the complete N^{th} degree polynomial for p_y^R, and to use the fictitious pressures in the region $-a \leq x \leq 0$ that are symmetric to those in the

region $0 \leq x \leq a$, as shown in Figure 3(b). By using this type of a fit, the coefficients A_n corresponding to the odd powers of x/a in Equation (14) automatically vanish, leaving only the even powers.

Crack Tip Location.- Because the finite element method analyzes the uncracked plate, the location of the crack tip needs to addressed. The simplest way to define the crack tip is to assume that the crack-tip coincides with an end node in the finite element model as shown in Figure 4(a). In this case the shaded elements are used to evaluate the tractions p_y^R in the crack region for a crack length of a_1 (see Figure 4(a)). The requirement that the crack tip coincide with a finite element node is, however, unnecessary. Figure 4(b) shows a slightly longer crack than in Figure 4(a), one whose tip does not coincide with a finite element node. In this situation one additional element needs to be used in the residual stress fit as shown by the shaded elements in Figure 4(b). This technique is similar to that used in the 3-D case in reference 8 where the elements on the crack plane do not conform to the exact shape of the elliptical or part-elliptical crack front.

EVALUATION OF THE FEAM

To evaluate the effectiveness of the finite-element-alternating method, the method is applied to a variety of mode-I problems for which accurate solutions are available. First, the method is applied to three commonly encountered fracture specimens with rectilinear boundaries. In this application the sensitivity of the solution to finite-element mesh refinement and the degree of polynomial fit to the residual pressures is studied. Next, the method is applied to a C-shaped edge cracked specimen to

evaluate its effectiveness when curved boundaries are involved. Third, the method is applied to problems involving stress concentrations. Last, some observations on the computational efficiency of the method are made.

In all cases plane strain conditions were assumed and a Poisson's ratio of 0.3 was used.

Specimens with Rectilinear Boundaries.- Figure 5 shows three common fracture specimens with rectilinear boundaries: center-cracked tension (CCT), single-edge cracked tension (SECT), and three-point bend specimen (TPB). The FEAM was applied to these specimens to evaluate the method. Because of symmetries one quarter of the CCT specimen and one half of the SECT and TPB specimens were considered in the analysis. Figure 6 shows both coarse and fine finite-element idealizations. The coarse mesh had 65 nodes and 16 elements; the fine mesh had 173 nodes and 48 elements. These two meshes were used to analyze both the CCT and SECT specimens with a crack with a/W ratio of 0.5.

Because of symmetry the v-displacements of all nodes along the $y = 0$ line were prescribed to be zero for both CCT and SECT specimens. For the CCT specimen the u-displacements of all nodes along the $x = 0$ line were prescribed to be zero. For the SECT specimen only one node is prescribed to have zero u-displacement to prevent rigid body motions. The boundaries that must be made traction free are: (1) $x = W$ and (2) $y = H$ for the CCT specimen and (1) $x = 0$, (2) $x = W$ and (3) $y = H$ for the SECT specimen. Therefore the [G] matrices of Equation (24) for the elements along these lines were calculated before the start of the iterative process.

Table 2 presents the normalized stress-intensity factors, $K/[S(\pi a)^{1/2}]$, obtained with the two meshes and for different degrees of

polynomial representation, N, in Equation (14). For the CCT specimen excellent accuracy was obtained even with only a quadratic representation (N=2) and the coarse (16-element) mesh. Furthermore, convergence to this accuracy, $(I_R/I_R^1) \leq 0.01$, was obtained with only 4 iterations. Figure 7 shows the convergence of the residual pressure for both CCT and SECT specimens. For the SECT specimen, on the other hand, a very good solution was obtained with N = 4 for the coarse mesh and with N = 5 for the fine mesh. The convergence to this accuracy was achieved with 11 iterations, which was much slower than with the CCT specimen. This was to be expected because the SECT specimen has an additional traction-free boundary (x = 0 line). Because accurate solutions for both specimens were produced with a polynomial of the fifth degree, N= 5 was used in the rest of the paper.

The use of a single fine mesh has a distinct advantage with this method. After the global stiffness matrix of the uncracked body is assembled and decomposed, a series of crack lengths can be analyzed in a single run. This is economical because the decomposition of the global stiffness matrix is the most expensive part of this method [4-8]. For each crack length, however, the [G] matrices of Equation (24) need to be computed. This procedure was followed to obtain stress-intensity factors for 6 crack lengths in a single run, for each of the CCT, SECT, and TPB specimens. The normalized stress-intensity factors and maximum crack-opening displacement (COD) for various a/W ratios are presented in Tables 3 and 4 for the CCT and SECT specimens,respectively. Tables 5 and 6 present the corresponding results for the TPB specimen. Reference results from the literature are also included in these tables for comparison. Excellent agreement was obtained for each of the five a/W ratios for each of the

configurations except for long cracks with an a/W ratio of 0.75. The maximum percent difference is observed to be about 12.5 percent for the stress-intensity factor. When the crack is long, a much finer mesh near the crack tip than that of Figure 6(b) is probably needed to obtain an accurate solution.

To ascertain that this is the case a new finite element model of the uncracked plate was developed and is shown in Figure 6(c). This model had 173 nodes and 48 elements as in Figure 6(b) but the mesh spacing is non-uniform in the x-direction. The stress-intensity factors were recomputed for the SECT specimen with this model for a/W ratios of 0.5, 0.625, and 0.75. Table 3 presents these results parenthetically. The new value of the normalized stress-intensity factor for a/W = 0.75 is now in excellent agreement with the reference value from the literature. The values for a/W=0.5 and 0.625 are about 3 percent lower than the reference value. This is expected because in the non-uniform model for a/W ratios of 0.5 and 0.625 the residual pressures were fit with stress values from 2 and 3 elements, respectively, while in the uniform model the fit was made from 4 and 5 elements. Thus, for a/W ratios up to 0.6, the uniform model performed well and for a/W ratio of 0.75 the non-uniform model gave accurate results. Therefore, a judicious choice of the uncracked finite element models is required to produce accurate stress-intensity factors with FEAM.

Recall that the results in Table 3 were obtained with an (I_R/I_R^1) ratio of 0.01. To study the effect of the termination value of (I_R/I_R^1), a more stringent value of 0.001 was used. The stress-intensity factors for the SECT specimen with a/W ratios of 0.5, 0.625, and 0.75 (with the uniform mesh , Figure 6(b)), were calculated to be 2.845, 4.620, and 9.536,

respectively. These values differed by less than one percent from the values given in Table 3. Therefore, a value of $(I_R/I_R^1) \leq 0.01$ was sufficient to produce converged values of stress-intensity factors and is used to terminate the algorithm in the rest of the paper.

Specimen with Curved Boundaries.- Figure 8(a) shows a C-shaped edge cracked specimen proposed by Kapp et. al [15]. This specimen was analyzed to evaluate the applicability of the method to problems involving curved boundaries. Figure 8(b) shows a finite element model of the uncracked body. Because of symmetries only the top half of the specimen was modeled. Because the pin holes and the region to the left of the pin are small and remote from the crack tip, they were not modeled. Figure 8(b) shows the finite element model which had 193 nodes and 54 elements. The curved boundaries in the specimen were modeled by piecewise linear segments.

The v-displacements of all nodes on the y = 0 line were prescribed zero. One node was constrained in the u-direction to prevent rigid body motion. A single concentrated load P was applied at node E of the model (see Figure 8(b)). The [G] matrices of Equation (24) were calculated for all elements along the curved boundaries BC and AD and along the straight boundary CD. As before the global stiffness matrix was assembled and stress-intensity factors for 6 normalized crack lengths ranging from a/W = 0.125 to 0.625 were calculated in a single run. Table 7 presents the normalized stress-intensity factors, $K/K(\alpha)$, where [15]

$$K(\alpha) = \frac{P}{W^{1/2}} (3(X/W) + 1.9 + 1.1\alpha) [1 + 0.25 (1-\alpha)^2 (1-r_1/r_2)]$$

with

$\alpha = a/W$ (See Figure 8(a)).

The present results are generally lower than the results of Kapp et. al [15] by about 4 percent. The accuracy of the results in ref. 15 is given

as ±1.5 percent. In the present analysis the pin holes and a small portion of the specimen were not modeled and the curved boundaries were modeled as piecewise linear, which may account for these small differences. The present results, however, indicate the applicability of the method to specimens with curved boundaries.

Specimens with Stress Concentrations.- To evaluate the FEAM in the presence of the additional complication of stress concentrations, two additional configurations have been analyzed (see Figure 9). The first configuration is that of two symmetric cracks emanating from a circular hole in a finite width plate subjected to remote tensile loading (Figure 9(a)). The second configuration is that of a crack emanating from a semi-circular notch in a finite width plate (Figure 9(b)) subjected to remote tensile loading.

Figure 10 presents the finite-element idealization of one quarter of the plate for the symmetric crack configuration and one-half of the plate for the semi-circular notch configuration. The finite-element model had 213 nodes and 60 elements. For both configurations the v-displacements on the y=0 line (AB in Figure 10) were prescribed to be zero. For the cracks from a hole, the u-displacements at all nodes on the line x = -R (line ED in Figure 10) were prescribed to be zero. For the crack from a notch, only one node was prescribed to have a zero u-displacement to prevent rigid body motions.

In both configurations the lines BC, CD, and EA had to be made stress free. Hence, the [G] matrices of all elements along these lines were calculated at the start of the iteration process. For the cracks from a circular hole, along the line DE symmetric boundary conditions require that the shear stresses be zero. To achieve this the [G] matrices of Equation

(24) for all elements along the line DE were calculated and the forces in the y-direction were used as the residual forces in Step 7 of the method. For the crack from a semi-circular notch, on the other hand, both x- and y-forces at all nodes along this line were used as the residual forces.

The stress-intensity factors were calculated for several crack lengths for each of these configurations in a single computer run. Tables 8 and 9 present the normalized stress-intensity factors for these configurations. They are compared with reference solutions from the literature [16,17]. Good agreement was obtained between the two sets of results. These results suggest that the FEAM can give accurate stress-intensity factors for problems involving stress-concentrations.

In all the examples analyzed so far the crack-tip in the original problem was always assumed to end at an end-node in the finite element model (see Figure 4(a)). As previously mentioned, this restriction can be removed by the technique suggested in Figure 4(b). To validate this technique, the problem of a crack from a semi-circular notch is analyzed with crack lengths that do not coincide with the finite-element nodal points. Table 10 presents the normalized stress-intensity factors obtained by this technique and compares them with those calculated by the boundary-force method [17]. When only one element is used to obtain p_y^R tractions and when the crack region is contained within this one element, the stress-intensity factors are not very accurate. However, when more than one element is used to model the crack region the results are within one percent of those from reference 17. These results suggest that for any crack length one could obtain the stress-intensity factors using a single fine mesh idealization provided that more than one element is used to model

the crack region.

Computer Program

The FEAM algorithm described here was written using FORTRAN 77 and was developed on a Personal Computer (PC) using a FORTRAN Compiler. The program was executed on personal computers with 8086, 80286, and 80386 microprocessors. Then the program was ported to a main frame computer with only one change in the source code. For the problem of two symmetric cracks from a circular hole (Figure 9(a)), the execution times on each of these computers for an analysis with six crack lengths (finite-element mesh with 213 nodes and 60 elements) are as follows.

Computer	PC-8086	PC-80286	PC-80386	CYBER 850
CPU Time (Minutes)	120	16	8	1.63

These computing times demonstrate the versatility of the method and show that one could obtain accurate stress-intensity solutions on personal computers with this method.

CONCLUDING REMARKS

A finite-element alternating method (FEAM) for two-dimensional crack configurations is presented. The method is based on an analytical solution for infinite plate containing a crack subjected to arbitrary normal tractions. The complete analytical solution for the infinite plate is given. The details of the FEAM are explained along with some computational aspects that improve the performance of the method.

The method is applied to several crack configurations for which reference stress-intensity factor solutions are available in the literature. Even though no attempt was made to optimize the finite element mesh, the method gave reasonably accurate stress-intensity factors and crack opening

displacements for all problems analyzed. A fifth-degree polynomial fit to the residual pressures was found to be sufficient.

Stress-intensity factors for several crack lengths were obtained in a single computer run with one finite-element idealization. The method can give a nearly continuous distribution of stress-intensity factors as a function of the crack length in a single computer run. The method was developed and implemented on a microcomputer (personal computer). The results demonstrate the feasibility of obtaining stress-intensity factors for a variety of cracked bodies on personal computers.

ACKNOWLEDGEMENT

The first author's contribution to this work was performed under NASA contract NAS1-18599 at the NASA Langley Research Center, Hampton ,Va.

REFERENCES

1. Tada, H., Paris, P. C, and Irwin, G. R., The Stress Analysis of Cracks Handbook, Del Research Corporation, Hellertown, Pa., 1973.

2. Rooke, D. P., and Cartwright, D. J., Compendium of Stress Intensity Factors, The Hillingdon Press, Uxbridge, Middx, 1976.

3. Sih, G. C., Handbook of Stress Intensity Factors, Volumes 1 & 2, Lehigh University, Bethelhem, Pa., 1973.

4. Murakami, Y., et al (Eds), Stress Intensity Factors Handbook, Volumes 1 & 2, Pergamon Press, 1987.

5. Nishioka, T., and Atluri, S. N., "Analytical Solution for Embedded Elliptical Cracks, and Finite Element-Alternating Method for Elliptical Surface Cracks, Subjected to Arbitrary Loadings," Engineering Fracture Mechanics, Vol 17, 1983, pp 247-268.

6. Nishioka, T., and Atluri, S. N., "An Alternating Method for Analysis of Surface Flawed Aircraft Structural Components," AIAA Jnl., Vol. 21, 1983, pp. 749-757.

7. Atluri, S. N., and Nishioka, T., "Computational Methods for Three-Dimensional Problems of Fracture," Chapter 7, In Computational Methods in Mechanics of Fracture, S. N. Atluri (Ed), North Holland, 1986, pp. 230-287.

8. Raju, I. S., Atluri, S. N., and Newman, J. C., Jr. "Stress-Intensity Factors for Small Surface and Corner Cracks in Plates," Paper Presented at the 20th National Symposium on Fracture Mechanics, Lehigh University, Bethlehem, Pa, June 23-25, 1987.

9. Sokolnikoff, I., Mathematical Theory of Elasticity, McGraw-Hill, Co., New York, 1956.

10. Kantorovich, L. V. and Krylov, V. I., Approximate Methods of Higher Analysis, Interscience, New York, 1964.

11. Isida, M., "Elastic Analysis of Cracks and Stress Intensity Factors", (in Japanese), Fracture Mechanics and Strength of Materials 2, Baifuukan, 1976, p. 128

12. Muskhelishvili, N. I., Some Basic Problems of the Mathematical theory of Elasticity, J. R. M. Radok (trans), Noordhoff, Groningen, The Netherlands, 1963.

13. Hinton, E., and Campbell, J. S., "Local and Global Smoothing of Discontinuous Finite Element Functions Using Least Squares Method,"

Int. Jnl. Num. Meth. Engng., Vol 8, 1974, pp. 461-480.

14. Hinton, E., and Campbell, J. S., "Local Least Squares Stress Smoothing for Parabolic Isoparametric Elements," Int. Jnl. Num. Meth. Engng., Vol. 9, 1975, pp. 235-256.

15. Kapp, J. A., Newman, J. C., Jr., and Underwood, J. H., " A Wide Range Stress Intensity Expression for the C-shaped Specimen," J. of Testing and Evaluation, Vol. 8, 1980, pp. 314-317.

16. Newman, J. C., Jr.," An Improved Method of Collocation for the Stress Analysis of Cracked Plates with Various Shaped Boundaries," NASA TN D-6376, 1971.

17. Tan, P. W., Raju, I. S., and Newman, J. C., Jr.," Boundary Force Method for Analyzing Two-dimensional Cracked Bodies", NASA TM 87725, May 1986.

Table. 1: Stress-intensity factors, K, and the COD at the center of a crack in an infinite plate subjected to arbitrary polynomial pressure distributions, $p_y = (x/a)^n$.

n	$\frac{K}{(\pi a)^{1/2}}$	$\frac{\mu\delta}{2(1-\nu)a}$ *
0	1	1
1	± 1/2	0
2	1/2	1/6
3	± 3/8	0
4	3/8	3/40
5	± 5/16	0
6	5/16	5/112
7	± 35/128	0
8	35/128	35/1152

The positive and negative signs in this table refer to the crack tips at x= ± a respectively. The negative values are meaningful only in the presence of additional forces which prevent crack closure.

* Note that $\frac{\mu\delta}{2(1-\nu)a} = \frac{K/(\pi a)^{1/2}}{n+1}$ for odd values of n

Table 2: Normalized stress-intensity factors, F_I, for the CCT and SECT specimens with coarse and fine meshes and with various degree of polynomial fits (a/W=0.5; H/W=2.5).

$$F_I = K/[S(\pi a)^{1/2}]$$

Degree of Polynomial fit, N	Coarse Mesh	Fine Mesh	Reference Value [1-4]
	CCT Specimen		
2	1.188(4)[a]	1.187(4)	
4	1.188(4)	1.187(4)	1.189
6	1.188(4)	1.187(4)	
	SECT Specimen		
2	2.964(13)	3.027(13)	
3	2.807(11)	2.918(11)	
4	2.808(11)	2.994(12)	2.828
5	2.752(11)	2.831(11)	
6	2.744(11)	2.800(11)	

[a]Values in the parentheses are the number of iterations required for convergence to one percent accuracy in the stress-intensity factors.

Table 3: Comparison of normalized stress-intensity factors, F_I, for the CCT and SECT specimens by the FEAM with accurate values from literature (H/W=2.5).

$$F_I = K/[S(\pi a)^{1/2}]$$

	a/W					
	0.125	0.25	0.375	0.5	0.625	0.75
CCT Specimen						
FEAM	1.009	1.039	1.094	1.187	1.342	1.626
Reference Value [1-4]	1.010	1.040	1.097	1.189	1.342	1.617
Percent Difference[a]	-0.01	-0.10	-0.27	-0.17	0.0	0.56
SECT Specimen						
FEAM	1.223	1.490	1.971	2.831 (2.757)[b]	4.587 (4.349)	9.447 (8.455)
Reference Value [1-4]	1.221	1.494	1.975	2.828	4.481	8.481
Percent difference	0.0	-0.27	-0.20	0.11 (-2.5)	2.4 (-3.0)	11.4 (-0.31)

[a] The percent difference here is based on (FEAM Value - Reference Value)/ Reference value.

[b] Values in the parenthesis were obtained with non-uniform mesh.

Table 4: Comparison of maximum normalized crack opening displacement, Δ_I, for the CCT and SECT specimens by the FEAM with accurate values from literature (H/W=2.5).

$$\Delta_I = E\delta/[4(1-\nu^2)Sa]$$

	a/W					
	0.125	0.25	0.375	0.5	0.625	0.75
CCT Specimen						
FEAM	1.009	1.039	1.093	1.181	1.324	1.569
Reference Value [1,4]	1.009	1.039	1.094	1.182	1.322	1.572
Percent Difference[a]	0.0	0.0	-0.09	-0.08	0.15	-0.19
SECT Specimen						
FEAM	1.546	1.988	2.922	4.925 (4.676)[b]	9.893 (9.148)	27.34 (23.94)
Reference Value [1-4]	1.605	2.044	2.986	4.922	9.649	23.04
Percent difference	-3.7	-2.7	-2.1	0.06 (-5.0)	2.5 (-5.2)	18.7 (3.2)

[a] The percent difference here is based on (FEAM Value - Reference Value)/ Reference value.

[b] Values in the parentheses were obtained with non-uniform mesh.

Table 5: Comparison of normalized stress-intensity factors, F_I, for the TPB specimen by the FEAM with accurate values from literature (H/W=2.5).

$$F_I = K/[(6P/W)(\pi a)^{1/2}]$$

	a/W					
	0.125	0.25	0.375	0.5	0.625	0.75
FEAM	0.970	0.992	1.123	1.408	2.030	3.759 (3.356)[b]
Reference Value [1-4]	0.977	1.007	1.137	1.416	1.981	3.349
Percent Difference[a]	-0.72	-1.5	-1.2	-0.56	-2.5	12.2 (0.21)

[a] The percent difference here is based on (FEAM Value - Reference Value)/ Reference value.

[b] Values in the parentheses were obtained with non-uniform mesh.

Table 6: Comparison of maximum normalized crack opening displacement, Δ_I, for the TPB specimen by the FEAM with accurate values from literature (H/W=2.5).

$$\Delta_I = E\delta / 4(1-\nu^2)Pa(6/W)]$$

	a/W					
	0.125	0.25	0.375	0.5	0.625	0.75
FEAM	1.344	1.548	2.009	2.955	5.128	12.17 (10.74)
Reference Value [4]	1.373	1.594	2.041	2.946	5.100	10.115
Percent Difference[a]	-2.1	-2.9	-1.6	0.31	0.55	20.3 (6.2)

[a] The percent difference here is based on (FEAM Value - Reference Value)/ Reference value.

[b] Values in the parentheses were obtained with non-uniform mesh.

Table 7: Comparison of normalized stress-intensity factors, $F(\alpha)$, for the C-shaped specimen by the FEAM with accurate values from the literature ($X/W = 0.5$; $r_2/r_1 = 2$; $\alpha = a/W$).

$$F(\alpha) = K/\{ P/(W^{1/2})(3X/W + 1.9 + 1.1\alpha)[1+0.25(1-\alpha)^2(1-r_1/r_2)] \}$$

	a/W					
	0.125	0.25	0.375	0.4375	0.5	0.625
FEAM	1.331	1.861	2.536	3.005	3.625	5.741
Reference Value [4,15]	1.316	1.942	2.650	3.120	3.733	5.777
Percent Difference[a]	1.1	-4.2	-4.3	-3.7	-2.9	-0.62

[a] The percent difference here is based on (FEAM Value - Reference Value)/ Reference value.

Table 8: Comparison of normalized stress-intensity factors, F_I, for two symmetric cracks from a circular hole by the FEAM with accurate values from literature (R/W = 0.25; c = R+a).

$$F_I = K/[S(\pi c)^{1/2}]$$

	F_I		
c/W	FEAM	Reference Value [16]	Percent Difference[a]
0.3	---	1.078	---
0.3125	1.088	(1.109)[b]	-1.9
0.375	1.203	(1.195)	0.7
0.4	---	1.216	---
0.4375	1.254	(1.240)	1.1
0.5	1.311	1.285	2.0
0.5417	1.355	(1.330)	1.9
0.583	1.405	(1.380)	1.8
0.6	---	1.397	---
0.667	1.528	(1.515)	0.86

[a] The percent difference here is based on (FEAM Value - Reference Value)/ Reference value.

[b] Values in the parentheses are interpolated values.

Table 9: Comparison of normalized stress-intensity factors, F_I, for a crack at a semi-circular notch by the FEAM with accurate values from literature (R/W = 0.25; c = R+a).

$$F_I = K/[S(\pi c)^{1/2}]$$

	F_I		
c/R	FEAM	Reference Value [17]	Percent Difference[a]
1.2	---	1.526	---
1.25	1.572	(1.605)[b]	-2.1
1.3	---	1.695	---
1.5	1.959	1.965	-0.3
1.75	2.336	2.336	0.0
2.0	2.836	2.818(2.827)[c]	0.6
2.167	3.273	3.255[c]	0.6
2.333	3.831	3.783[c]	1.2
2.667	5.549	5.409[c]	2.6
3.00	9.102	8.481[c]	7.3

[a] The percent difference here is based on (FEAM Value - Reference Value)/ Reference value.

[b] Values in the parentheses are interpolated values.

[c] Values correspond to an edge crack in a plate without the notch. For $c/R \geq 2$, the effect of the notch is insignificant.

Table 10: Comparison of normalized stress-intensity factors, F_I, for a crack at a semi-circular notch by the FEAM when the crack tip does not coincide with finite-element nodes (R/W = 0.25; c = R+a).

$$F_I = K/[S(\pi c)^{1/2}]$$

	F_I		
c/R	FEAM	Reference Value [17]	Percent Difference[a]
1.125(1)[b]	1.413	1.350	4.6
1.150(1)	1.481	1.407	5.2
1.200(1)	1.551	1.526	1.66
1.375(2)	1.776	1.790	-0.77
1.400(2)	1.807	1.825	-0.96

[a] The percent difference here is based on (FEAM Value - Reference Value)/ Reference value.

[b] The values in the parentheses are the number of elements in the crack region.

LIST OF FIGURE CAPTIONS

Fig. 1: Crack in an infinite plate subjected to two normal concentrated forces.

Fig. 2: Procedure used in the alternating method.

Fig. 3: Fictitious pressure extrapolations.

Fig. 4: Elements used in determining the residual pressures for different length cracks.

Fig. 5: Specimens with rectilinear boundaries.

Fig. 6: Finite-element idealizations used for specimens with rectilinear boundaries.

Fig. 7: Convergence of the residual pressures for CCT and SECT specimens.

Fig. 8: C-shaped specimen and a finite-element idealization

Fig. 9: Crack problems with stress concentrations

Fig. 10: Finite-element model for problems with stress concentrations.

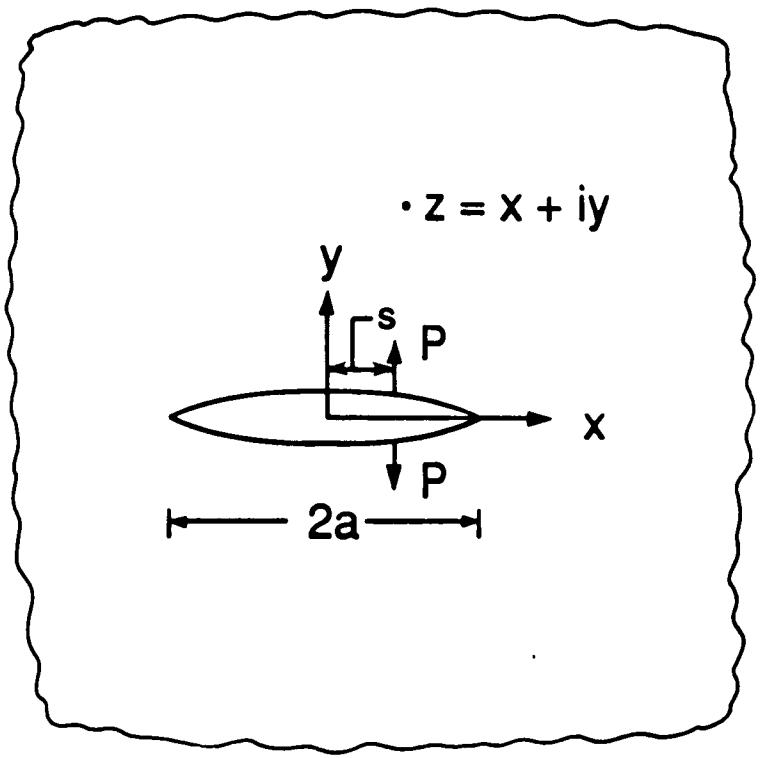

Fig. 1: Crack in an infinite plate subjected to two normal concentrated forces.

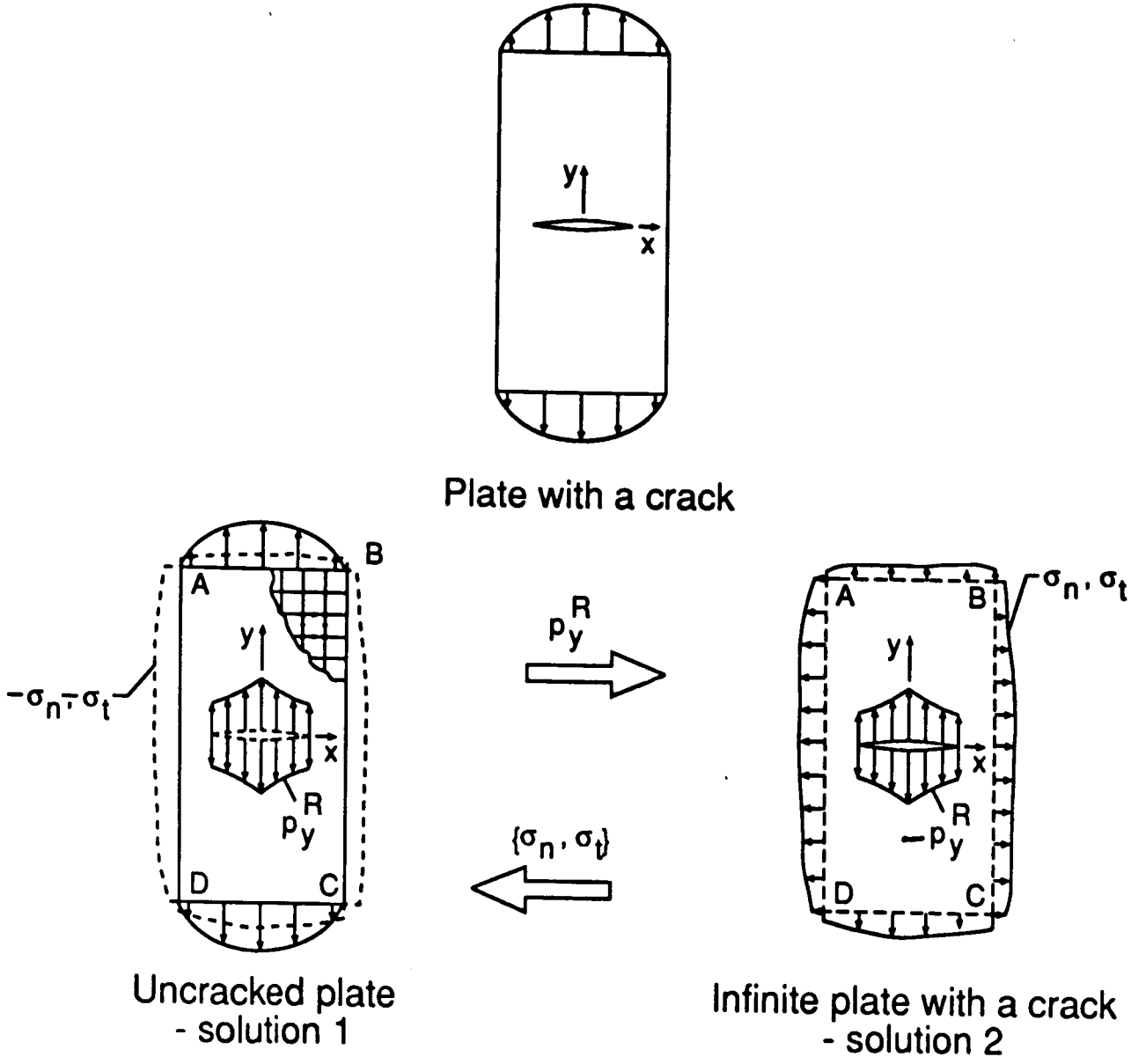

Fig. 2: Procedure used in the alternating method.

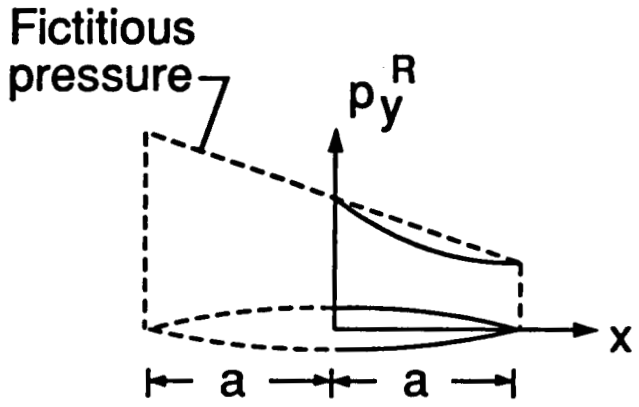

(a) Residual pressures for edge cracks.

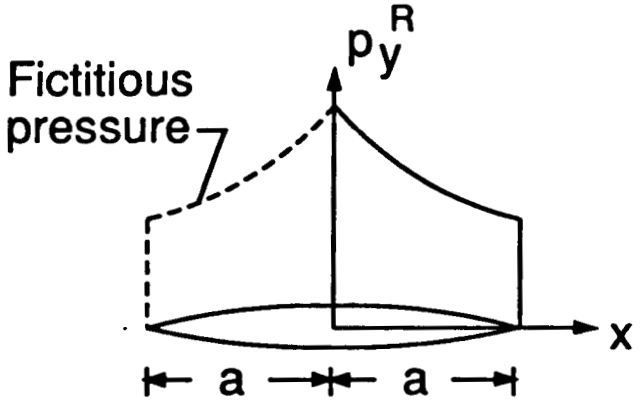

(b) Residual pressures for crack configurations that are symmetric about x = 0 line.

Fig. 3: Fictitious pressure extrapolations.

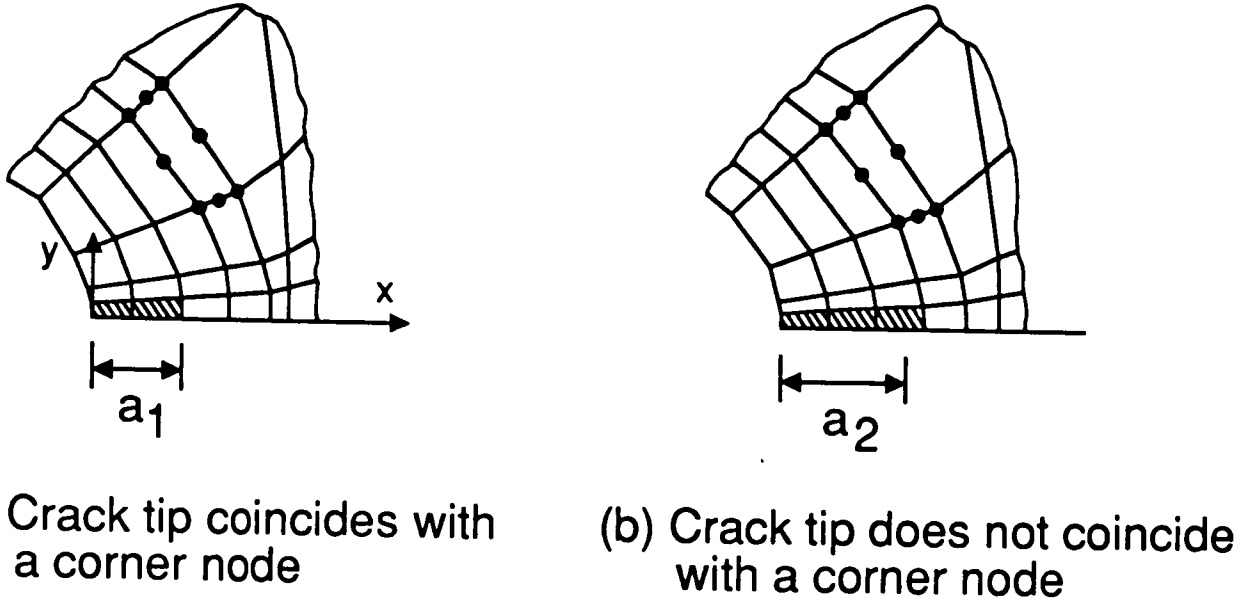

Fig. 4: Elements used in determining the residual pressures for different length cracks.

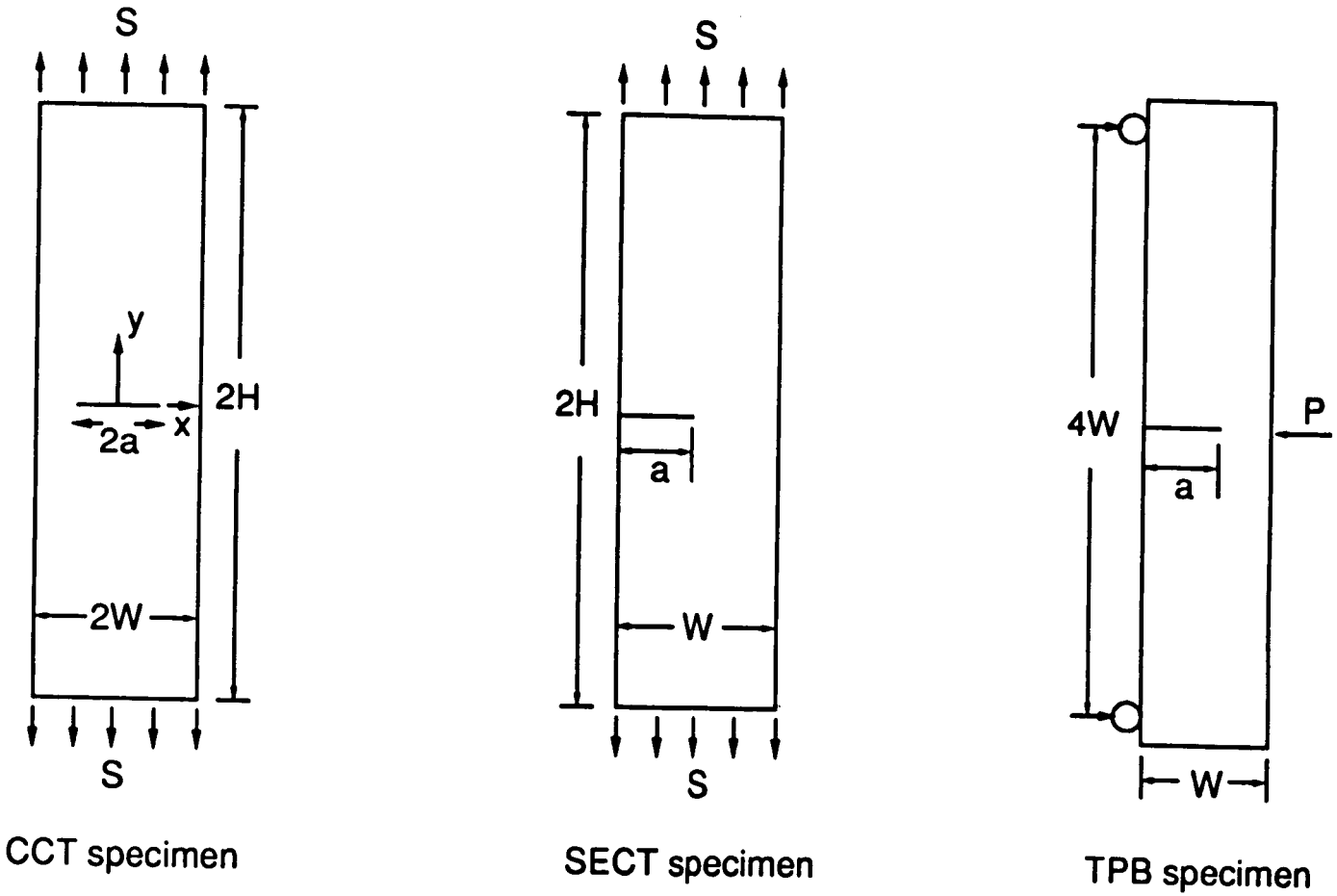

Fig. 5: Specimens with rectilinear boundaries. (H/W=2.5)

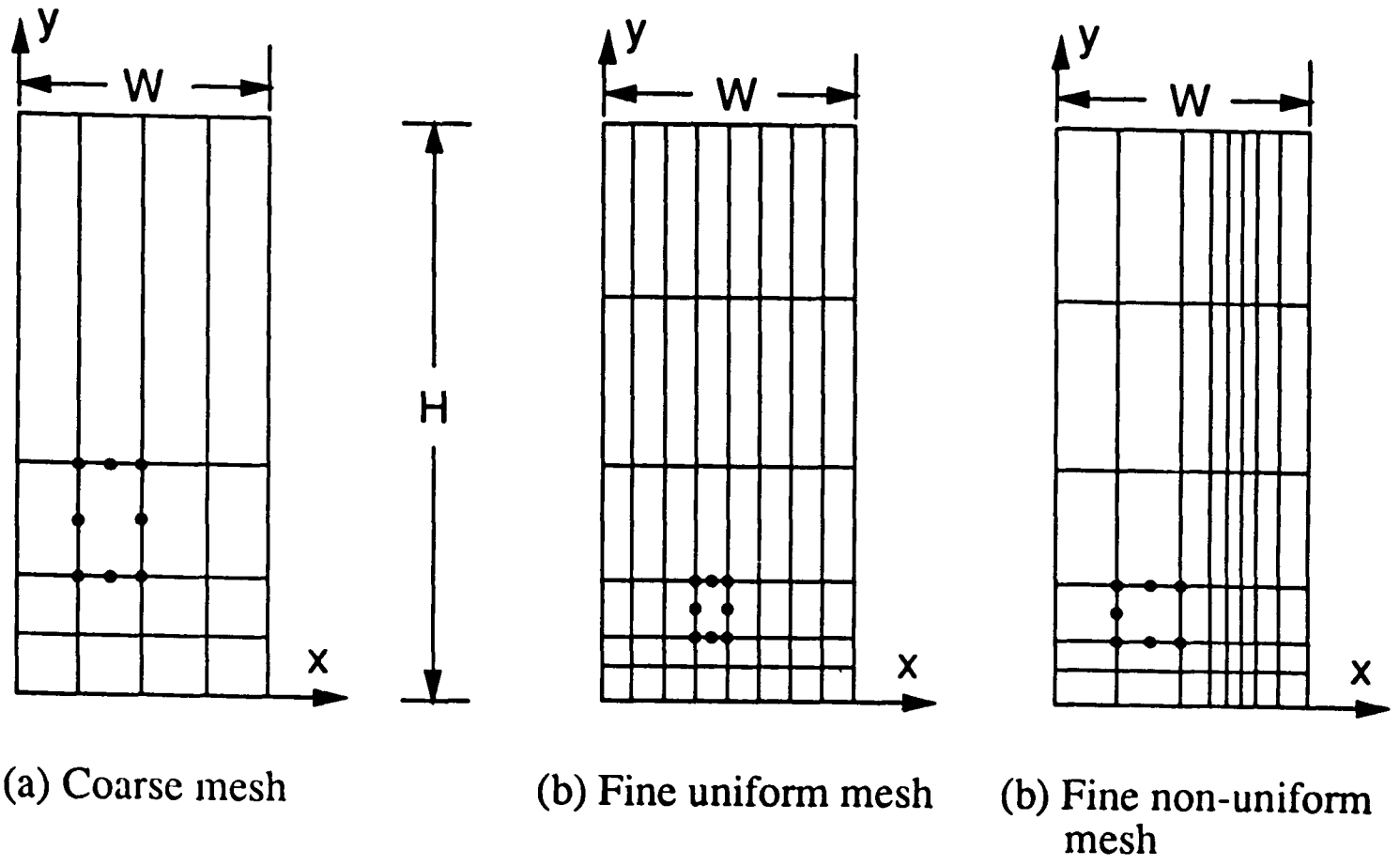

Fig. 6: Finite-element idealizations used for specimens with rectilinear boundaries.

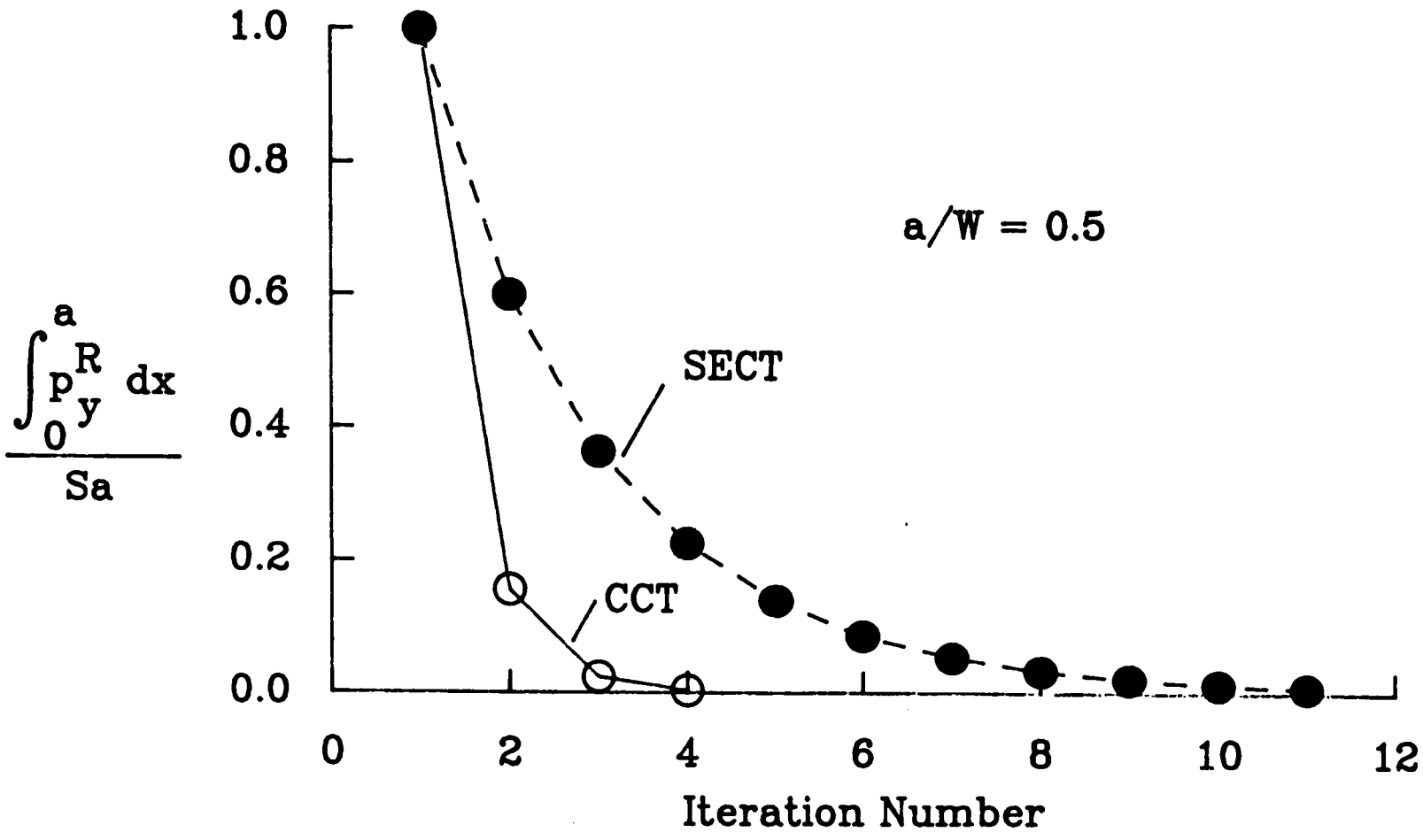

Fig. 7: Convergence of the residual pressures for CCT and SECT specimens.

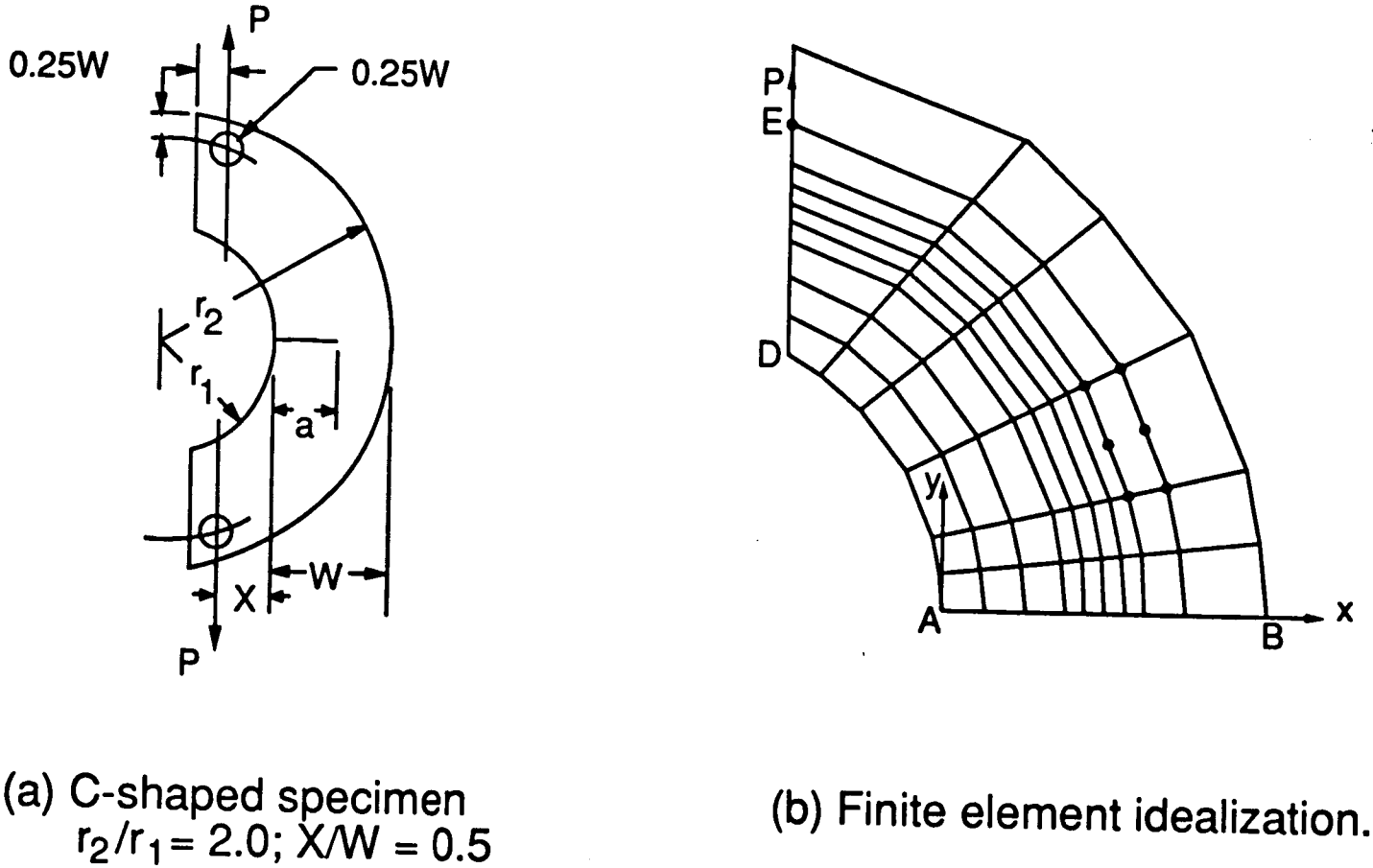

(a) C-shaped specimen
$r_2/r_1 = 2.0$; $X/W = 0.5$

(b) Finite element idealization.

Fig. 8: C-shaped specimen and a finite-element idealization

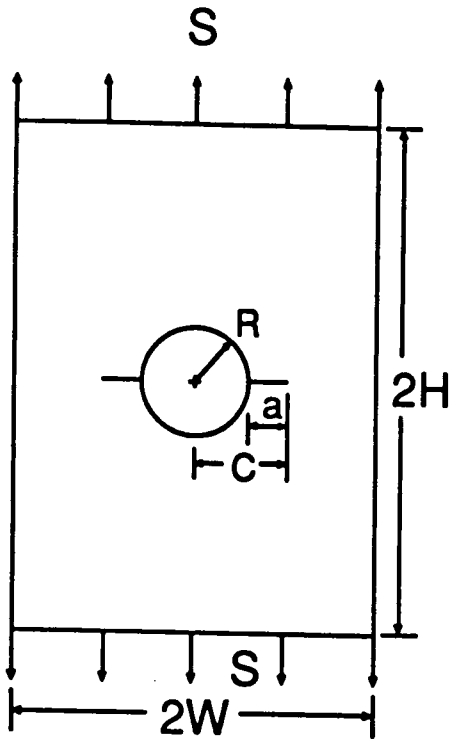

(a) Cracks from a circular hole.

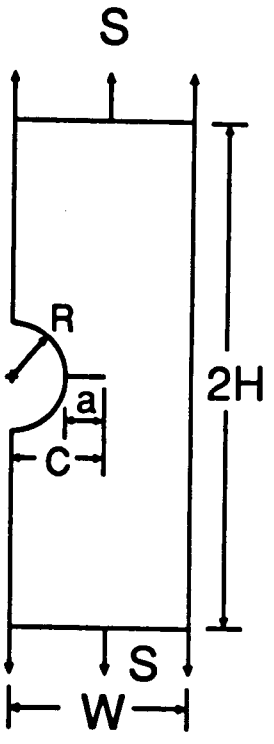

(b) Cracks from a semi-circular notch

Fig. 9: Crack problems with stress concentrations
(R/W=0.25, H/W=2.0)

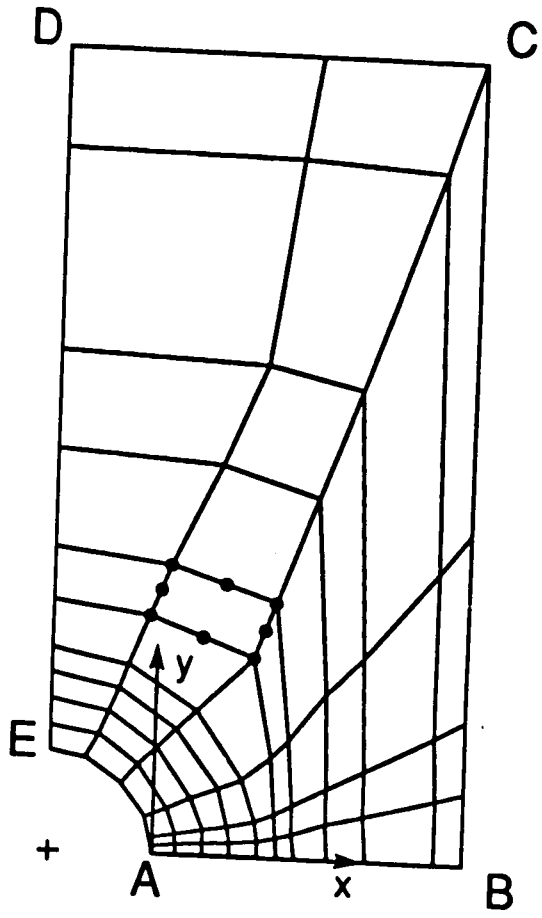

Fig. 10: Finite-element model for problems with stress concentrations.

NASA National Aeronautics and Space Administration

Report Documentation Page

1. Report No.	2. Government Accession No.	3. Recipient's Catalog No.
NASA TM-100616		

4. Title and Subtitle
A Finite-Element Alternating Method for Two-Dimensional Mode-I Crack Configurations

5. Report Date
May 1988

6. Performing Organization Code

7. Author(s)
I. S. Raju and W. B. Fichter

8. Performing Organization Report No.

10. Work Unit No.
506-43-41-02

9. Performing Organization Name and Address
NASA Langley Research Center
Hampton, VA 23665-5225

11. Contract or Grant No.

13. Type of Report and Period Covered
Technical Memorandom

12. Sponsoring Agency Name and Address
National Aeronautics and Space Administration
Washington, DC 20546-0001

14. Sponsoring Agency Code

15. Supplementary Notes
I. S. Raju: Analytical Services and Materials, Inc., Hampton, Virginia.
W. B. Fichter: Langley Research Center, Hampton, Virginia.

16. Abstract
A finite-element alternating method is presented for two-dimensional mode-I crack problems. An analytical solution for an arbitrary polynomial normal pressure distribution applied to the crack faces is obtained and used as the basic solution in the method. The method is applied to several crack problems to study its efficiency and the results are compared to accurate stress-intensity factor solutions in the literature. The method gave reasonably accurate stress-intensity factors and crack opening displacements with minimal computing effort. Because the method must model only the uncracked body, finite-element models with many degrees of freedom are not warranted and therefore, the method has been implemented on personal computers.

17. Key Words (Suggested by Author(s))
Finite-element alternating method
Two-dimensional mode-I crack problems
Stress-intensity

18. Distribution Statement
Unclassified-Unlimited

Subject Category 39

19. Security Classif. (of this report)	20. Security Classif. (of this page)	21. No. of pages	22. Price
Unclassified	Unclassified	46	A03